AGU PUBLICATIONS

Geophysical Research Letters

RESEARCH LETTER
10.1002/2017GL073363

Key Points:
- Exactly dated tree ring chronologies are used to reconstruct wet season rainfall over the southern Amazon Basin from 1799 to 2012, a 150 year extension of the short instrumental record
- Atmospheric circulation associated with equatorward surges of extratropical air leads to higher rainfall over the southern Amazon in both instrumental and reconstructed data
- The magnitude of reconstructed decadal droughts and pluvials increased after 1950

Supporting Information:
- Data S1

Correspondence to:
D. Stahle,
dstahle@uark.edu

Citation:
Lopez, L., D. Stahle, R. Villalba, M. Torbenson, S. Feng, and E. Cook (2017), Tree ring reconstructed rainfall over the southern Amazon Basin, *Geophys. Res. Lett.*, *44*, doi:10.1002/2017GL073363.

Received 13 MAR 2017
Accepted 3 JUL 2017
Accepted article online 10 JUL 2017

Tree ring reconstructed rainfall over the southern Amazon Basin

Lidio Lopez[1], David Stahle[2], Ricardo Villalba[3], Max Torbenson[2], Song Feng[2], and Edward Cook[4]

[1]IANIGLA-CONICET, Mendoza, Argentina, [2]Department of Geosciences, University of Arkansas, Fayetteville, Arkansas, USA, [3]Instituto Argentino de Nivología, Glaciología y Ciencias Ambientales (IANIGLA), Mendoza, Argentina, [4]LDEO, Columbia University, New York, New York, USA

Abstract Moisture sensitive tree ring chronologies of *Centrolobium microchaete* have been developed from seasonally dry forests in the southern Amazon Basin and used to reconstruct wet season rainfall totals from 1799 to 2012, adding over 150 years of rainfall estimates to the short instrumental record for the region. The reconstruction is correlated with the same atmospheric variables that influence the instrumental measurements of wet season rainfall. Anticyclonic circulation over midlatitude South America promotes equatorward surges of cold and relatively dry extratropical air that converge with warm moist air to form deep convection and heavy rainfall over this sector of the southern Amazon Basin. Interesting droughts and pluvials are reconstructed during the preinstrumental nineteenth and early twentieth centuries, but the tree ring reconstruction suggests that the strong multidecadal variability in instrumental and reconstructed wet season rainfall after 1950 may have been unmatched since 1799.

1. Introduction

Instrumental precipitation and streamflow data indicate an increase in hydroclimatic variability over the Amazon Basin during the last 45 years [*Callède et al*., 2004, *Gloor et al*., 2013]. Two of the most severe droughts yet recorded in Amazonia occurred in 2005 and 2010 [*Lewis et al*., 2011; *Marengo et al*., 2011], while in 2012 record flooding was observed in western Amazonia simultaneously with extreme drought in northeastern Brazil [*Marengo et al*., 2013]. In 2014 and 2015 summer rainfall was 100% above normal in portions of the southern Amazon Basin and caused record flooding on the Madeira and Branco Rivers [*Espinoza et al*., 2014; *Marengo and Espinoza*, 2016]. In fact several "once in century" hydrological extremes have occurred in just the past decade on the Amazon River, including five extreme floods and two extreme low flows [*Marengo and Espinoza*, 2016]. These hydroclimatic changes have included more extreme streamflow seasonality, with lower minimum flows and higher maximum flows [*Gloor et al*., 2013]. This apparent amplification of the hydrologic cycle has been hypothesized to arise from both natural and anthropogenic factors, including interactions between deforestation and climate over the Amazon [*Gentry and Lopez-Parodi*, 1980, *Callède et al*., 2004, *Chagnon and Bras*, 2005, *Khanna et al*., 2017], anthropogenic alterations to global climate [*Li et al*., 2006, *Malhi et al*., 2008], and increased water vapor transport from the tropical North Atlantic [*Gloor et al*., 2013].

A decline in annual precipitation is predicted for the 21st century over most of Amazonia based on Coupled Model Intercomparison Project Phase 5 (CMIP5) climate model ensemble simulations under business-as-usual greenhouse gas emissions and land cover changes [*Feng and Fu*, 2013]. Other climate simulations suggest that a decrease in anthropogenic aerosols along with the increase in greenhouse gases will lead to further increases in hydroclimatic extremes over the Amazon [*Cox et al*., 2008]. Remote sensing of tropical precipitation and vegetation over the Amazon Basin indicates that deforestation leads to less efficient moisture recycling and that current trends in Amazonian deforestation may result in 12 to 21% declines in wet and dry season precipitation over Amazonia, respectively [*Spracklen et al*., 2012]. Just how unprecedented these recent and predicted hydroclimate changes might be in the context of natural climate variability is difficult to determine from the few instrumental records that begin at Manaus with measurements of precipitation in 1901 [*Garreaud et al*., 2009] and with streamflow on the Rio Negro in 1902 [e.g., *Richey et al*., 1989]. In fact, the entire 7.5×10^6 km^2 drainage basin of the Amazon River, nearly as large as the coterminous United States, has only three precipitation records that date back to 1901 and modern Amazonian weather stations are still very sparsely distributed [*Garreaud et al*., 2009].

Proxy records of hydroclimatic variability from the Amazon Basin are available and under development [*Maslin and Burns*, 2000; *Strikis et al*., 2011; *Wang et al*., 2017], but notably absent are long climate sensitive tree ring chronologies, even though 16,000 tree species may be native to the lowland forests of the Amazon [*ter Steege et al*., 2013]. It is remarkable that the most species-rich forest ecosystem in the world, the rainforests of Amazonia [*Gentry*, 1988], have not produced a single well-replicated, independently validated, multicentury tree ring chronology useful for exact dating or climate reconstruction. However, strong precipitation seasonality does exist over some sectors of the Amazon Basin and exactly dated, well-replicated tree ring chronologies have recently been developed from upland sites in the southern portion of the basin. These include a regional network of nine moisture sensitive ring width chronologies of *Centrolobium microchaete* in the southern Amazon Basin of eastern Bolivia [*Lopez and Villalba*, 2011], based on over 200 individual trees with anatomically distinctive annual growth bands that have been dated to the calendar year of formation using dendrochronology. Seven of the nine chronologies are significantly correlated over their 70 year common interval, and the two that are not correlated may have suffered human impacts on the growth record (especially fire and logging).

Here we describe the strong regional wet season moisture signal detected in the longest and most highly correlated subset of four *Centrolobium* chronologies and use them to reconstruct wet season precipitation totals from 1799 to 2012. This is the first well-replicated annually resolved, preinstrumental reconstruction of precipitation yet reported in the southern Amazon, and it is used to place the hydroclimatic changes of the last 50 years into a longer historical perspective. The results indicate that the *Centrolobium* chronologies provide outstanding proxies of regional rainfall and the continental-scale climate dynamics responsible for wet season rainfall variability in the relative short instrumental record from the southern Amazon sector. Subdecadal droughts and pluvials are reconstructed during the nineteenth and early twentieth centuries, but the dramatic multidecadal variability in instrumental and reconstructed wet season precipitation after 1950 is unmatched in this reconstruction since 1799.

2. Data and Methods

Cross sections of *C. microchaete* were cut opportunistically from recently felled trees in legal logging concessions in the tropical seasonally dry *Chiquitano* forests of eastern Bolivia over the period 2005 to 2010 [*Lopez and Villalba*, 2011]. Full or partial cross sections are often essential for the dendrochronology of tropical hardwood species with highly complex cellular anatomy of the annual growth layers. Increment cores rarely provide sufficient surface area for definitive annual ring identification, especially in slow growing old trees with microscopic rings [*Stahle et al*., 1999]. The internal correlation of ring width series from individual trees at each site, the length of the chronology, the correlation of the derived ring width chronology among sites, and the strength of the wet season precipitation signal in each chronology were all used to identify the four best *C. microchaete* chronologies for precipitation reconstruction.

The ring width data from the four sites represent 152 dated radii from 97 separate trees that were detrended and standardized using the ARSTAN computer program [*Cook and Krusic*, 2005]. The raw ring width data were power transformed, and an age-dependent spine was used to remove nonclimatic effects on radial growth and to standardize the mean and variance of each individual ring width time series [*Cook and Peters*, 1981; *Melvin et al*., 2007]. The standard ring width chronologies were entered into principal component analysis to summarize the common growth signal among the four chronologies. The first PC explains 75.2% of the four site growth variance (1925–2006), and the amplitude time series on the first PC was compared with regional precipitation data to define the optimum precipitation season for reconstruction. The Climatic Research Unit (CRU) 0.5° gridded monthly precipitation data set CRU TS3.10 was used in this analysis [*Harris et al*., 2014]. The CRU precipitation data for the southern Amazon extend back to 1901, but the gridded data before the middle twentieth century can suffer from the complete loss of nearby station observations in remote regions of the study area. The grid point data for wet season precipitation (October–March) over the southern Amazon region exhibiting the highest correlations with the first PC of tree growth were extracted from CRU TS3.10 and averaged to provide the predictand for reconstruction from tree rings (the coordinates of the extracted region are 13.75–17.25°S and 61.25–63.25°W). These correlations with CRU precipitation data were restricted to the period 1971–2005 to define the response and optimal region.

The reconstruction was computed with a nested principal components regression procedure and includes four separate segments (or nests) linked continuously from 1799 to 2006. The reconstruction is based on the single Purubí chronology from 1799 to 1833, two chronologies from 1834 to 1899 (Purubí and Concepcion), three from 1900 to 1923 (Purubí, Concepcion, and Santa Monica (which was truncated to 1900)), and four from 1924 to 2006 (Purubí, Concepcion, Santa Monica, and Palestina). The instrumental precipitation totals for the October to March wet season were then used to extend the reconstruction forward another 6 years from 2007 to 2012. The detrended and standardized ring width chronologies from all four sites were used without autoregressive modeling of the predictors or predictand. Semiparametric 90% prediction intervals, based on a combination of standard least squares theory [*Seber and Lee*, 2003; *Olive*, 2007] and the use of the maximum entropy bootstrap method [*Vinod*, 2006] to randomly perturb the predictors and predictands, were computed to estimate uncertainties over time in the nested reconstructions [*Cook et al*., 2013]. As part of the generation of the semiparametric prediction intervals, estimates of regression model interpolations and extrapolations are generated from the Hat matrix of predictors and are used to identify those extrapolated values in the reconstruction likely to be least reliable for interpretation [*Wiesberg*, 1985]. Singular spectrum analysis (SSA) [*Ghil et al*., 2002; *St. George and Ault*, 2011] was performed to identify important frequency components in the 214 year reconstruction.

The observed and reconstructed precipitation data were compared with instrumental geopotential heights and 1000–700 hPa water vapor flux to examine the possible large-scale forcing of wet season precipitation over the southern Amazon region during the calibration period. The atmospheric circulation and humidity data were obtained from the NCEP/NCAR Reanalysis (National Centers for Environmental Prediction/National Center for Atmospheric Research Reanalysis v1) [*Kalnay et al*., 1996]. The rainfall data were also correlated with the global sea surface temperature field [*Huang et al*., 2015], indices of the El Niño–Southern Oscillation (Multivariate ENSO Index, MEI) [*Wolter and Timlin*, 2011], the Interdecadal Pacific Oscillation (Tripole Index) [*Henley et al*., 2015], and an index of the Southern Annular Mode (SAM) developed by *Marshall* [2003] and now available from 1957 to present (also referred to as the Antarctic Oscillation).

3. Results and Discussion

The first PC of tree growth is most highly correlated with wet season precipitation totals (October–March) over a large sector of the southern Amazon Basin of eastern Bolivia and southwestern Brazil (Figure 1a). This area is located in the headwaters of the Madeira River, the largest tributary of the Amazon and the fifth largest river in the world. The area of wet season precipitation correlation also crosses the drainage divide from the Amazon into the Rio Paraguay Basin to the south. Over 75% of mean annual precipitation occurs during the 6 month wet season from October to March in the region of the southern Amazon depicted in Figure 1a and extracted from the CRU TS3.10 data set for reconstruction. The precipitation signal recorded by the tree ring chronologies spans the entire summer wet season. The tree ring data are positively correlated with monthly precipitation totals from October to April, significantly for all months except October and February ($p < 0.05$; 1965–2006). The highest single monthly correlation is computed for January ($r = 0.56$), which is on average the wettest month of the year (Figure 1c). Summer precipitation variability in the study area is strongly influenced on daily timescales by interactions between the South American Summer Monsoon (SASM) and incursions of cold and dry extratropical air into the southern Amazon Basin [*Garreaud and Wallace*, 1998; *Marengo and Rogers*, 2001; *Hurley et al*., 2015]. These dynamics appear to be involved in our analyses of both instrumental and reconstructed rainfall on seasonal timescales.

The reconstructions were calibrated on the period 1965–2006 when the regionally averaged precipitation data appear to be of highest quality (Figure 1b) and are also well correlated with the individual tree ring chronologies. However, none of the nested reconstructions could be successfully validated against the regional average CRU precipitation data before 1965. Instead, the instrumental data were divided from 1965 to 2006 into two subperiods for experimental validation of the tree ring estimates of wet season precipitation (Table 1). All four nested subsets of tree ring data can be reasonably calibrated and verified during the short subperiods of 1965–1983 and 1984–2006 (and other subdivisions of 1965–2006), and for this reason the full 42 year period from 1965 to 2006 was used to calibrate the final reconstructions presented in Figure 2. These nested reconstruction models represent from 36 to 51% of the variance in instrumental wet season precipitation totals, based on the single to four chronology subsets, respectively (Table 1). The reduction of error

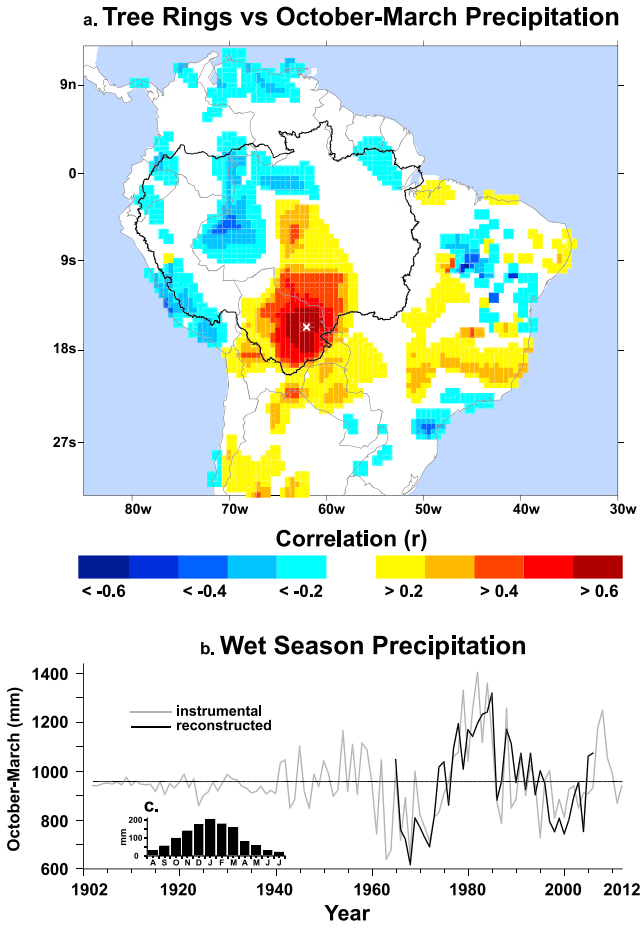

Figure 1. (a) The regional tree ring data are correlated with the 0.5° CRU TS3.10 gridded precipitation data averaged for the October–March wet season over tropical South America for the period 1971–2005 (i.e., the amplitude time series from the first principal component of four tree ring chronologies from eastern Bolivia (x)). Note the positive correlations over the southern Amazon Basin of Bolivia and western Brazil (drainage basin of the Amazon River indicated by black line). (b) The October–March wet season precipitation totals for the southern Amazon region are plotted from 1902 to 2012 for the instrumental data and 1965 to 2006 for the tree ring reconstruction. Note the attenuation of instrumental precipitation variance prior to circa 1950 due to limited observations. (c) The monthly mean precipitation amounts computed for the period 1965–2012 are also plotted.

statistic calculated with a leave-one-out procedure during the calibration period (calibration period cross-validation reduction of error (CVRE); Table 1) is positive for all four models and provides one measure of the skill involved with the nested calibrations based on the full 1965–2006 period. The Hat matrix of predictors estimated as part of the semiparametric prediction intervals indicate only four probable extrapolations (1808, 1840, 1868, and 1985 exceed the 0.1 threshold; not shown), in spite of the decline in tree ring chronology predictors associated with each nested reconstruction model and the reduction in sample size within these chronologies.

The instrumental and reconstructed precipitation data are plotted together in Figure 1b and illustrate the agreement at interannual and especially decadal scales. This agreement is reflected in the statistics presented in Table 1, and even the nested subset based on only one tree ring chronology explains 36% of the variance in the instrumental data during the 1965–2006 calibration period (Table 1). The decadal component is a dominant feature of instrumental precipitation over the southern Amazon, and the reconstruction reproduces the decade-long droughts of the late 1960s and 1990s and the pluvial of the 1970–1980s. However, the skill of the reconstruction is not only based on coherent decadal variability. The first difference time series of both instrumental and reconstructed October–March precipitation, free of decadal excursions and trend, are correlated at $r = 0.41$ ($p < 0.01$; 1952–2006).

The reconstruction is not correlated with the CRU precipitation data prior to 1965 ($r = -0.19$; 1902–1964). This loss of signal is related in part to the complete absence of precipitation observations before 1943 in the reconstructed grid box and the reduction in stations from the larger region available for gridding into the study area before 1950. The gridded CRU precipitation data set was filled with climatological mean values when nearby station observations were not available [*Harris et al.*, 2014]. This gridding strategy extends the precipitation data back to 1901 but can attenuate the variance of selected grid point precipitation when observations are scarce (e.g., prior to 1950; Figure 1b). Consequently, the reliability of the tree ring reconstruction prior to 1950 was also checked against a few instrumental hydroclimatic time series that are available from the southern Amazon region during the early twentieth century. For example, the reconstruction is weakly correlated with October–March precipitation totals recorded at Santa Cruz, Bolivia, from 1925 to 1950, but using just a 4 month wet season (November–February), the correlation with this single station is

Table 1. Calibration Validation and Results are Listed for the Four Nested Principal Components Regression Models Used to Reconstruct October–March Precipitation Totals in the Southern Amazon Basin[a]

NEST	Calibrate	Validate	R^2_{adj}	CVRE	RSQ	RE	CE
Four Chronologies	1965–2006		0.51	0.50			
INP-PAL-PUR-SMO	1965–1983	1984–2006	0.61		0.39	0.25	0.23
	1984–2006	1965–1983	0.39		0.61	0.55	0.54
Three Chronologies	1965–2006		0.50	0.49			
INP-PUR-SMO	1965–1983	1984–2006	0.59		0.42	0.27	0.26
	1984–2006	1965–1983	0.42		0.58	0.52	0.52
Two Chronologies	1965–2006		0.42	0.40			
INP-PUR	1965–1983	1984–2006	0.45		0.39	0.33	0.32
	1984–2006	1965–1983	0.39		0.44	0.43	0.42
One Chronology	1965–2006		0.36	0.34			
PUR	1965–1983	1984–2006	0.40		0.35	0.20	0.19
	1984–2006	1965–1983	0.35		0.40	0.34	0.33

[a]The four chronologies used were Inpa-Concepcion, Palestina, Purubi, and Santa Monica, all located in eastern Bolivia (coordinates = 16.32904°S–61.61400°W, 16.21824°S–61.66284°W, 15.96766°S–62.22718°W, and 15.63916°S–62.41079°W, respectively). The reconstructions are all based on the full calibration period 1965–2006, and the subperiod calibration and validation results are also listed for each model (R^2_{adj} = coefficient of determination adjusted for loss of degrees of freedom, CVRE = calibration period cross-validation reduction of error, RSQ = Pearson correlation coefficient squared for the verification period, RE = reduction of error, CE = coefficient of efficiency). The Durbin-Watson test for autocorrelation of residuals is not significant for all calibrations.

$r = 0.63$ ($p < 0.001$) during the 26 year precalibration interval. The reconstruction is also significantly correlated with the level of the Paraguay River recorded at Ladario, Paraguay, for the period 1901–1950 ($r = 0.41$; $p < 0.01$). These correlations prior to the calibration period help substantiate the dating accuracy and proxy climate value of the reconstruction. For comparison, the grid box average CRU October–March precipitation totals are correlated with minimum water levels in the Paraguay River from 1965 to 2006 ($r = 0.54$) and from 1951 to 1964 ($r = 0.36$) but are not from 1901 to 1950 ($r = -0.03$). The grid box average precipitation totals are correlated with the single Santa Cruz station record for October–March from 1965 to 2006 at $r = 0.42$ and from 1951 to 1964 at $r = 0.39$. But the correlation drops to $r = 0.26$ for the period 1926 to 1950 (the Santa Cruz station began observations in 1926). This loss of regional hydroclimate signal in the CRU grid box average wet season precipitation data before 1950 and the absence of correlation between the reconstructed precipitation data and the CRU regional precipitation average prior to 1950 both highlight the value of the reconstruction, which is providing over 150 years of new wet season rainfall data for the poorly instrumented southern Amazon Basin.

The nested reconstruction is plotted in Figure 2 along with the significant SSA waveforms identified in the time series. Subdecadal to decadal droughts are estimated by the nested reconstructions during the first decade of the 1800s, the 1820s, and 1890s, and pluvials are estimated during the 1840s, 1870–1980s, and early 1900s (Figure 2a). These reconstructed regimes do not equal the magnitude or duration of drought during the 1960s or the pluvial during the 1970–1980s (Figures 1b and 2), but they do indicate, not surprisingly, that subdecadal and decadal variability was a feature of hydroclimatic variability over the southern Amazon during the nineteenth and early twentieth centuries.

The reconstruction is dominated by interannual variability, but spectral analysis indicates that subdecadal, decadal, and multidecadal modes of variability are important components of the reconstruction and might reflect forcing from various internal and potentially external climate dynamics. The subdecadal component with a periodicity of 4.7 years that represents 11.4% of the reconstructed variance is plotted in Figure 2b. The amplitude of this subdecadal component varies over the past 214 years but is most important from approximately 1890–1940. The reconstruction is not strongly or consistently correlated with indices of the El Niño/Southern Oscillation (ENSO), but the subdecadal component might nonetheless reflect some regional precipitation response to ENSO forcing. A decadal component is identified with a period of 10.9 years that represents 16.9% of the reconstructed variance (Figure 2c). The amplitude of the decadal component is strongest before 1850 when the reconstruction is based on the fewest tree ring series. A multidecadal component of variability is also identified in the reconstruction with a period of 28.5 years representing a third of the variance in the reconstruction (34.5%). The multidecadal component of variability increased substantially

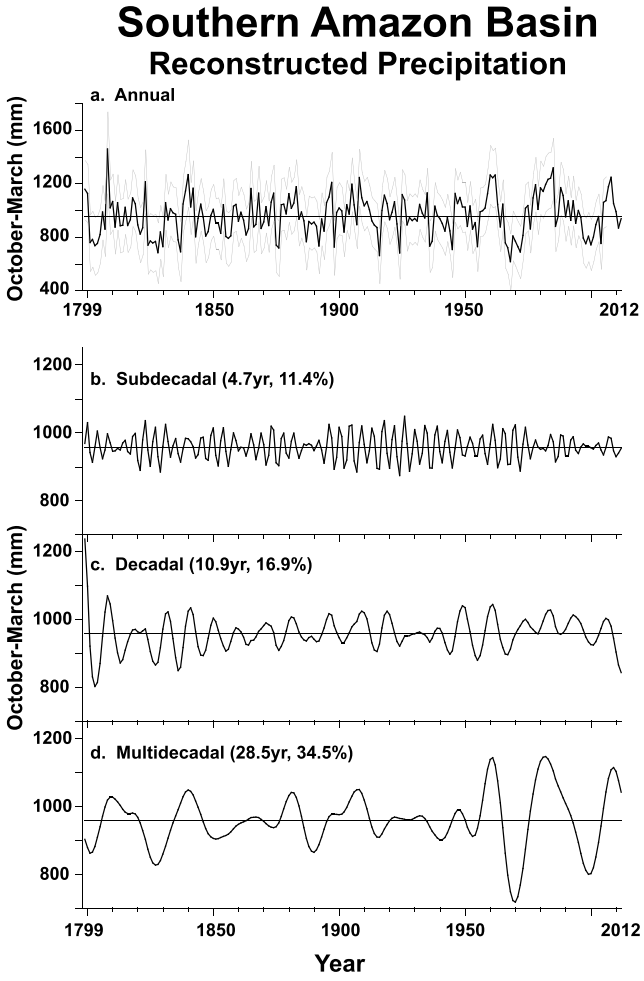

Figure 2. (a) The tree ring reconstructed wet season rainfall totals for the southern Amazon Basin are plotted from 1799 to 2012 along with the 0.05 and 0.95 semiparametric prediction intervals. The SSA waveforms for the (b) subdecadal, (c) decadal, and (d) multidecadal components of reconstructed rainfall are also illustrated.

after 1950 (Figure 2d), reflecting more intense and prolonged droughts and pluvials, which may be part of the hydroclimatic changes seen more broadly across the Amazon [e.g., *Marengo and Espinoza*, 2016].

Comparisons with the atmospheric circulation field indicate that the reconstructions faithfully reproduce the large-scale climate dynamics associated with instrumental rainfall variations over the southern Amazon (Figure 3). In regression analyses, instrumental and reconstructed wet season rainfall are both strongly and positively associated with the 700 hPa geopotential height field over midlatitude South America (Figures 3a and 3b). This strong low-level anticyclonic circulation favors the advection of cold extratropical air into the southern Amazon sector (especially in Figure 3b). The equatorward edge of these extratropical surges of low-level moisture (1000–700 hPa) collides with warm moist tropical air from the Atlantic, in large bands of deep convection that enhance summer rainfall over the southern Amazon. These results are consistent with previous studies indicating that summer precipitation variability in the area is strongly influenced on daily timescales by interactions between the South American Summer Monsoon and incursions of cold relatively dry extratropical air into the southern Amazon [*Garreaud and Wallace*, 1998; *Marengo and Rogers*, 2001; *Hurley et al*., 2015]. The organized bands of deep convection caused by the intrusion of cooler air from the extratropics may produce between 25 and 50% of the total summer rainfall over the southern Amazon [*Garreaud and Wallace*, 1998] and over 70% of the total summertime (December, January, February) snow accumulation on the Quelccaya Ice Cap, Peru [*Hurley et al*., 2015]. The regression results in Figure 3 therefore suggest that excess wet season rainfall may largely reflect an accumulation of the daily convection dynamics associated with incursions of extratropical air that appear to intensify the SASM in this sector of the southern Amazon [*Hurley et al*., 2015].

The instrumental and reconstructed records of wet season precipitation over the southern Amazon study area do not exhibit strong and consistent relationships with ENSO, as noted in previous studies of instrumental summer rainfall from the area [e.g., *Garreaud et al*., 2009; *Espinoza et al*., 2014] or with indices of the Interdecadal Pacific Oscillation. The instrumental and reconstructed wet season records are also not strongly or consistently correlated with SSTs in the Atlantic, which have been linked with precipitation over the western Amazon during the dry season [*Fernandes et al*., 2015]. The instrumental and reconstructed precipitation data are correlated with SSTs in the Humboldt Current sector of the extreme southeastern Pacific (not shown), but these correlations may simply be the consequence of the strong correlation with anticyclonic flow over midlatitude South America (Figure 3).

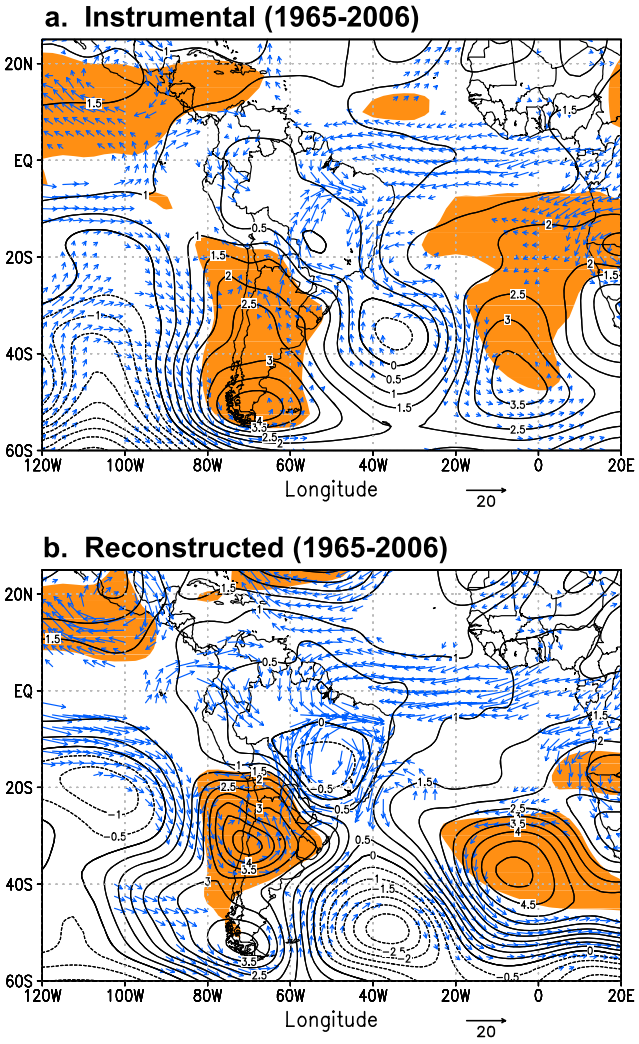

Figure 3. The vertically integrated October–March water vapor flux (arrows) and 700 hPa geopotential height (contours) regressed against the October–March (a) instrumental and (b) reconstructed precipitation from the southern Amazon Basin study area during the 1965–2006 period. Water vapor flux is in units of kg/m/S (only significant fluxes are plotted (95% confidence level; note 1 sigma wind-scale vector)). Orange shading indicates areas where the correlation between geopotential height and precipitation is significant at 95% level. The contour interval is 0.5 gpm.

There is some evidence for a teleconnection between southern Amazon precipitation and middle- to high-latitude circulation associated with the Southern Annular Mode, which is the most important extratropical circulation feature in the Southern Hemisphere [*Jones and Widmann*, 2004]. The zonal mean October–March geopotential heights for 1000–100 hPa were regressed against the October–March instrumental and reconstructed precipitation from the study area for 1965–2006. There is an out-of-phase pattern between the Antarctic and midlatitude Southern Hemisphere confined to the middle to lower troposphere (not shown), reflecting the apparent relationship between southern Amazon precipitation and the SAM.

The teleconnection between wet season precipitation in the southern Amazon and the SAM is, however, highly nonstationary, as has been noted in analyses of midlatitude South American precipitation by *Silvestri and Vera* [2009]. Reconstructed precipitation over the southern Amazon is positively correlated with the January average SAM index [*Marshall*, 2003] from 1957 to 1981 (r = +0.47; $p < 0.05$) but becomes negatively correlated from 1982 to 2006 ($r = -0.73$, $p < 0.001$). The instrumental October–March precipitation data for the southern Amazon are not correlated with the January SAM index before 1981 (r = +0.07 for 1957–1981) but become negatively correlated for 1982–2006 at −0.47 ($p < 0.05$). *Silvestri and Vera* [2009] report a similar change in the sign of correlations between the SAM index and instrumental precipitation over a larger sector of southern South America.

4. Conclusions

The calibration statistics indicate that the *Centrolobium* tree ring chronologies provide high-quality proxies of October–March wet season precipitation totals, which represent over 75% of the average annual rainfall in this highly seasonal moisture regime of the southern Amazon Basin (e.g., Figure 1c). But these tree ring proxies also faithfully represent the continental-scale climate dynamics responsible for deep convection and higher warm season rainfall over the southern Amazon. This includes anticyclonic circulation in the lower troposphere over midlatitude South America that favors the intrusion of cooler drier air into the southern Amazon where it converges with moist tropical air and results in organized bands of deep convection

responsible for a significant fraction warm season rainfall. Although the new rainfall record is only 214 years long, which is relatively short for dendroclimatic reconstructions, the gridded instrumental precipitation data for the reconstructed area suffer from limited station observations before 1950. The reconstruction therefore adds some 150 years of new hydroclimatic information to help clarify the nature and causes of rainfall variability over the southern Amazon.

The recent large increase in the multidecadal variability of wet season rainfall totals over the southern Amazon is an important feature of the new tree ring reconstruction. These decadal changes in wet season moisture are clearly evident after 1965 in the instrumental rainfall data for the southern Amazon (Figure 1b) and in the annual mean stream levels of the Madeira River that drains this region [*Marengo and Espinoza*, 2016]. Decadal droughts and pluvials are present in the reconstruction during the nineteenth and early twentieth centuries, but they are not estimated to have been as severe and sustained as those observed and reconstructed after 1950. The new tree ring reconstruction therefore suggests that the increase in multidecadal variability may be part of the hydroclimatic changes documented during recent decades over Amazonia with instrumental data, and they may have been unprecedented since 1799. The successful rainfall reconstruction based on *Centrolobium* demonstrates that these hypotheses can be tested with the development of additional tree ring proxies of wet season rainfall across the Amazon.

Acknowledgments
This research has been supported by National Science Foundation Paleo Perspectives on Climate Change (P2C2) award AGS-1501321 CONICET-Argentina, and the Inter-American Institute for Global Change Research (CRN II 2047). We thank Toby Ault, Ana Carolina Barbosa, Roel Breinen, Dan Griffin, Jochen Schongart, and Scott St. George for assistance. Three anonymous reviewers provided valuable suggestions that improved this article. The raw ring width data, standardized ring width chronologies, instrumental precipitation data, and the derived precipitation reconstruction are all available from the supporting information (Data S1) and from the International Tree Ring Data Bank at the NOAA Paleoclimatology Program: https://www.ncdc.noaa.gov/data-access/paleoclimatology-data and upon request from the authors (dstahle@uark.edu). Lamont-Doherty Earth Observatory contribution 8130.

References

Callède J., J. L. Guyot, J. Ronchail, Y. L'Hôte, and H. N. E. de Oliveira (2004), Evolution du débit de l'Amazone à Óbidos de 1903 à 1999 / Evolution of the River Amazon's discharge at Óbidos from 1903 to 1999, *Hydrol. Sci. J.*, *49*, 85–97.

Chagnon F. J. F., and R. L. Bras (2005), Contemporary climate change in the Amazon, *Geophys. Res. Lett.*, *32*, L13703, doi:10.1029/2005GL022722.

Cook, E. R., and K. Peters (1981), The smoothing spline: A new approach to standardizing forest interior tree-ring width series for dendroclimatic studies, *Tree-Ring Bull.*, *41*, 45–53.

Cook, E. R., and P. J. Krusic (2005), Program ARSTAN: A tree-ring standardization program based on detrending and autoregressive time series modeling, with interactive graphics. Manuscript on file, Tree-Ring Lab, Lamont Doherty Earth Obs. of Columbia Univ., Palisades, New York.

Cook, E. R., J. G. Palmer, M. Ahmed, C. A. Woodhouse, P. Fenwick, M. U. Zafar, M. Wahab, and N. Khan (2013), Five centuries of upper Indus River flow from tree rings, *J. Hydrol.*, *486*, 365–375.

Cox, P. M., P. P. Harris, C. Huntingford, R. A. Betts, M. Collins, C. D. Jones, T. E. Jupp, J. A. Marengo, and C. A. Nobre (2008), Increasing risk of Amazonian drought due to decreasing aerosol pollution, *Nature*, *453*, 212–215.

Espinoza, J. C., J. A. Marengo, J. Ronchail, J. M. Carpio, L. N. Flores, and J. L. Guyot (2014), The extreme 2014 flood in south-western Amazon basin: The role of tropical-subtropical South Atlantic SST gradient, *Environ. Res. Lett.*, *9*, 124007.

Feng, S., and Q. Fu (2013), Expansion of global drylands under a warming climate, *Atmos. Chem. Phys.*, *13*, 10,081–10,094.

Fernandes, K., A. Giannini, L. Verchot, W. Baethgen, and M. Pinedo-Vasquez (2015), Decadal covariability of Atlantic SSTs and western Amazon dry-season hydroclimate in observations and CMIP5 simulations, *Geophys. Res. Lett.*, *42*, 6793–6801, doi:10.1002/2015GL063911.

Garreaud, R. D., and J. M. Wallace (1998), Summertime incursions of midlatitude air into subtropical and tropical South America, *Mon. Weather Rev.*, *126*, 2713–2733.

Garreaud, R. D., M. Vuille, R. Compagnucci, and J. Marengo (2009), Present-day South American climate, *Palaeogeogr. Palaeoclimatol. Palaeoecol.*, *281*, 180–195.

Gentry, A. H., and J. Lopez-Parodi (1980), Deforestation and increased flooding of the Upper Amazon, *Science*, *210*, 1354–1356.

Gentry, A. H. (1988), Changes in plant community diversity and floristic composition on environmental and geographical gradients, *Ann. Missouri Bot. Garden*, *75*, 1–34.

Ghil, M., et al. (2002), Advanced spectral methods for climatic time series, *Rev. Geophys.*, *40*(1), 1003, doi:10.1029/2000RG000092.

Gloor, M., R. J. W. Brienen, D. Galbraith, T. R. Feldpausch, J. Schongart, J. L. Guyot, J. C. Espinoza, J. Lloyd, and O. L. Phillips (2013), Intensification of the Amazon hydrological cycle over the last two decades, *Geophys. Res. Lett.*, *40*, 1729–1733, doi:10.1002/grl.50377.

Harris, I., P. D. Jones, T. J. Osborn, and D. H. Lister (2014), Updated high resolution grids of monthly climatic observations—The CRU TS3.10 dataset, *Int. J. Climatol.*, *34*, 623–642.

Huang, B., V. F. Banzon, E. Freeman, J. Lawrimore, W. Liu, T. C. Peterson, T. M. Smith, P. W. Thorne, S. D. Woodruff, and H.-M. Zhang (2015), Extended reconstructed sea surface temperature version 4 (ERSST.v4). Part I: Upgrades and intercomparisons, *J. Clim.*, *28*, 911–930, doi:10.1175/JCLI-D-14-00006.1.

Henley, B. J., J. Gergis, D. J. Karoly, S. Power, J. Kennedy, and C. K. Folland (2015), A Tripole Index for the Interdecadal Pacific Oscillation, *Clim. Dyn.*, *45*, 3077–3090.

Hurley, J. V., M. Vuille, D. R. Hardy, S. J. Burns, and L. G. Thompson (2015), Cold air incursions, $\delta^{18}O$ variability, and monsoon dynamics associated with snow days at Quelccaya ice cap, Peru, *J. Geophys. Res. Atmos.*, *120*, 7467–7487, doi:10.1002/2015JD023323.

Jones, J. M., and M. Widmann (2004), Atmospheric science: Early peak in the Antarctic Oscillation Index, *Nature*, *432*, 290–291.

Kalnay, E., et al. (1996), The NCEP/NCAR 40-year reanalysis project, *Bull. Am. Meteorol. Soc.*, *77*, 437–471.

Khanna, J., D. Medvigy, S. Fueglistaler, and R. Walko (2017), Regional dry-season climate changes due to three decades of Amazonian deforestation, *Nat. Clim. Change*, *7*, 200–204.

Lewis, S. L., P. M. Brando, O. L. Phillips, G. M. F. van der Heijden, and D. Nepstad (2011), The 2010 Amazon drought, *Science*, *331*, 554.

Li, W. H., R. Fu, and R. E. Dickinson (2006), Rainfall and its seasonality over the Amazon in the 21st century as assessed by the coupled models for the IPCC AR4, *J. Geophys. Res.*, *111*, D02111, doi:10.1029/2005JD006355.

Lopez, L., and R. Villalba (2011), Climate influences on the radial growth of Centrolobium microchaete, a valuable timber species from tropical dry forests in Bolivia, *Biotropica*, *43*, 41–49, doi:10.1111/j.1744-7429.2010.00653.x.

Malhi, Y., J. T. Roberts, R. A. Betts (2008), Climate change and the fate of the Amazon, *Science*, *319*, 169–172.
Marengo, J. A., and J. C. Rogers (2001), Polar air outbreaks in the Americas: Assessments and impacts during modern and past climates, in *Interhemispheric Climate Linkages*, edited by V. Markgraf, pp. 31–51, Academic Press, San Diego, Calif.
Marengo, J. A., J. Tomasella, L. M. Alves, W. Soares, and D. A. Rodriguez (2011), The drought of 2010 in the context of historical droughts in the Amazon region, *Geophys. Res. Lett.*, *38*, L12703, doi:10.1029/2011GL047436.
Marengo, J. A., L. M. Alves, W. R. Soares, D. A. Rodriguez, H. Camargo, M. P. Riveros, and A. D. Pablo (2013), Two contrasting severe seasonal extremes in tropical South America in 2012: Flood in Amazonia and drought in northeast Brazil, *J. Clim.*, *26*, 9137–9154.
Marengo, J. A., and J. C. Espinoza (2016), Extreme seasonal droughts and floods in Amazonia: Causes, trends and impacts, *Int. J. Climatol.*, *36*, doi:10.1002/joc.4420.
Marshall, G. J. (2003), Trends in the southern annular mode from observations and reanalyses, *J. Clim.*, *16*, 4134–4143.
Maslin, M. A., and S. J. Burns (2000), Reconstruction of the Amazon basin effective moisture availability over the past 14,000 years, *Science*, *290*, 2285–2287.
Melvin, T. M., K. R. Briffa, K. Nicolussi, and M. Grabner (2007), Time-varying-response smoothing, *Dendrochronologia*, *25*, 65–69.
Olive, D. J. (2007), Prediction intervals for regression models, *Comput. Stat. Data Anal.*, *51*, 3115–3122.
Richey, J. E., C. Nobre, and C. Deser (1989), Amazon River discharge and climate variability: 1903 to 1985, *Science*, *246*, 101–103.
St. George, S., and T. R. Ault (2011), Is energetic decadal variability a stable feature of the central Pacific Coast's winter climate?, *J. Geophys. Res.*, *116*, D12102, doi:10.1029/2010JD015325.
Seber, G. A. F., and A. J. Lee (2003), *Linear Regression Analysis*, 2nd ed., Wiley-Interscience, New York.
Silvestri, G., and C. Vera (2009), Nonstationary impacts of the southern annular mode on southern hemisphere climate, *J. Clim.*, *22*, 6142–6148.
Spracklen, D. V., S. R. Arnold, and C. M. Taylor (2012), Observations of increased tropical rainfall preceded by air passage over forests, *Nature*, *489*, 282–285.
Stahle, D. W., P. T. Mushove, M. K. Cleaveland, F. Roig, and G. A. Haynes (1999), Management implications of annual growth rings in *Pterocarpus angolensis* from Zimbabwe, *For. Ecol. Manage.*, *124*, 217–229.
Strikis, N. M., F. W. Cruz, H. Cheng, I. Karmann, R. L. Edwards, M. Vuille, X. Wang, M. S. de Paula, V. F. Novello, and A. S. Auler (2011), Abrupt variations in south American monsoon rainfall during the Holocene based on a speleothem record from central-eastern Brazil, *Geology*, *39*, 1075–1078.
ter Steege, H., et al. (2013), Hyperdominance in the Amazonian tree flora, *Science*, *342*, 325–334.
Vinod, H. D. (2006), Maximum entropy ensembles for time series inference in economics, *J. Asian Econ.*, *17*, 955–978, doi:10.1016/j.asieco.2006.09.001.
Wang, X., R. L. Edwards, A. S. Auler, H. Cheng, X. Kong, Y. Wang, F. W. Cruz, J. A. Dorale, and H. W. Chiang (2017), Hydroclimatic changes across the Amazon lowlands over the past 45,000 years, *Nature*, *541*, 204–207.
Wiesberg, S. (1985), *Applied Linear Regression*, 2nd ed., John Wiley, New York.
Wolter, K., and M. S. Timlin (2011), El Nino/Southern Oscillation behaviour since 1871 as diagnosed in an extended multivariate ENSO index (MEI.ext), *Int. J. Climatol.*, *31*, 1074–1087, doi:10.1002/joc.2336.